Senescent epithelial cells remodel the microenvironment for the progression of oral submucous fibrosis through secreting TGF-β1

Zijia Wang [1] , **Ying Han** [1] , **Ying Peng** [1] , **Shuhui Shao** [1] , **Huanquan Nie** [1] , **Kun Xia** [2] , **Haofeng Xiong** [Corresp., 1, 3, 4, 5] , **Tong Su** [Corresp. 1, 3, 4, 5]

[1] Department of Oral and Maxillofacial Surgery, Center of Stomatology, Xiangya Hospital, Central South University, Changsha, Hunan, China

[2] Center for Medical Genetics & Hunan Key Laboratory of Medical Genetics, School of Life Sciences, Central South University, Changsha, Hunan, China

[3] Research Center of Oral and Maxillofacial Tumor, Xiangya Hospital, Central South University, Changsha, China

[4] Institute of Oral Precancerous Lesions, Central South University, Changsha, China

[5] National Clinical Research Center for Geriatric Disorders, Xiangya Hospital, Changsha, China

Corresponding Authors: Haofeng Xiong, Tong Su
Email address: xionghaofeng@sklmg.edu.cn, sutong@csu.edu.cn

Objectives: Cellular senescence is strongly associated with fibrosis and tumorigenesis. However, whether the epithelium of oral submucous fibrosis (OSF) undergoes premature senescence remains unclear. This study investigates the roles of senescent epithelial cells in OSF. **Methods:** The immunohistochemistry and Sudan black B staining were performed to identify epithelium senescence in OSF tissues. Arecoline was used to induce human oral keratinocytes (HOKs) senescence. The cell morphology, senescence-associated β galactosidase activity, cell counting Kit 8, immunofluorescence, quantitative real-time PCR, and western blot assay were used to identification of senescent HOKs. The enzyme-linked immunosorbent assay was exerted to evaluate the levels of transforming growth factor β1 (TGF-β1) in the supernatants of HOKs treated with or without arecoline. **Results:** The senescence-associated markers, p16 and p21, were overexpressed in OSF epithelium. These expressions were correlated with alpha-smooth actin (α-SMA) positively and proliferating cell nuclear antigen (PCNA) negatively. Moreover, Sudan black staining showed that there was more lipofuscin in OSF epithelium. In vitro, HOKs treated with arecoline showed senescence-associated characteristics including enlarged and flattened morphology, senescence-associated β galactosidase staining, cell growth arrest, γH2A.X foci, upregulation of p53, p21, and TGF-β1 protein levels. Moreover, senescent HOKs secreted more TGF-β1. **Conclusions:** Senescent epithelial cells are involved in OSF progression and may become a promising target for OSF treatment.

1 **Senescent epithelial cells remodel the microenvironment for the progression of oral submucous**
2 **fibrosis through secreting TGF-β1**

4 Zijia Wang[1], Ying Han[1], Ying Peng [1], Shuhui Shao[1], Huanquan Nie[1], Kun Xia[5], Haofeng Xiong[1, 2, 3, 4, *], Tong
5 Su[1, 2, 3, 4, *]

7 1. Department of Oral and Maxillofacial Surgery, Center of Stomatology, Xiangya Hospital, Central South
8 University, Changsha, Hunan, 410008, China

9 2. Research Center of Oral and Maxillofacial Tumor, Xiangya Hospital, Central South University,
10 Changsha, Hunan, 410008, China

11 3. Institute of Oral Precancerous Lesions, Central South University, Changsha, Hunan, 410008, China

12 4. National Clinical Research Center for Geriatric Disorders, Xiangya Hospital, Changsha, Hunan, 410008,
13 China

14 5. Center for Medical Genetics & Hunan Key Laboratory of Medical Genetics, School of Life Sciences,
15 Central South University, Changsha, Hunan, 410008, China

17 *Corresponding author: Tong Su, M.D., Department of Oral and Maxillofacial Surgery, Center of
18 Stomatology, Xiangya Hospital, Central South University, NO.87 Xiangya Road, Changsha, Hunan,
19 410008, China (email: sutong@csu.edu.cn); Haofeng Xiong, Center of Stomatology, Xiangya Hospital,
20 Central South University, NO.87 Xiangya Road, Changsha, Hunan, 410008, China (email:
21 xionghaofeng@sklmg.edu.cn)

24   **Abstract**

25   **Objectives:** Cellular senescence is strongly associated with fibrosis and tumorigenesis. However,
26   whether the epithelium of oral submucous fibrosis (OSF) undergoes premature senescence remains
27   unclear. This study investigates the roles of senescent epithelial cells in OSF.

28   **Methods:** The immunohistochemistry and Sudan black B staining were performed to identify
29   epithelium senescence in OSF tissues. Arecoline was used to induce human oral keratinocytes (HOKs)
30   senescence. The cell morphology, senescence-associated β galactosidase activity, cell counting Kit 8,
31   immunofluorescence, quantitative real-time PCR, and western blot assay were used to identification
32   of senescent HOKs. The enzyme-linked immunosorbent assay was exerted to evaluate the levels of
33   transforming growth factor β1 (TGF-β1) in the supernatants of HOKs treated with or without
34   arecoline.

35   **Results:** The senescence-associated markers, p16 and p21, were overexpressed in OSF epithelium.
36   These expressions were correlated with alpha-smooth actin (α-SMA) positively and proliferating cell
37   nuclear antigen (PCNA) negatively. Moreover, Sudan black staining showed that there was more
38   lipofuscin in OSF epithelium. In vitro, HOKs treated with arecoline showed senescence-associated
39   characteristics including enlarged and flattened morphology, senescence-associated β galactosidase
40   staining, cell growth arrest, γH2A.X foci, upregulation of p53, p21, and TGF-β1 protein levels.
41   Moreover, senescent HOKs secreted more TGF-β1.

42   **Conclusions:** Senescent epithelial cells are involved in OSF progression and may become a promising
43   target for OSF treatment.

44

45   **Keywords:** Oral submucous fibrosis, epithelial cell, cellular senescence, senescence-associated
46   secretory phenotype, transforming growth factor β1

47

1. Introduction

Oral submucous fibrosis (OSF) is a premalignant mucosal disease with inflammation and progressive fibrosis. Although OSF is a multifactorial disease, epidemiological studies indicated that betel nut chewing is one of the most significant risk factors for OSF (Angadi & Rekha 2011; Tilakaratne et al. 2006). During betel nut chewing, its physical and chemical stimuli directly impose on oral mucosa. Among these adverse stimuli, arecoline is a recognized chemical pathogenic factor for OSF, mainly activating fibroblasts to promote the collagen deposition and suppress the collagen degradation (Yang et al. 2021).As fibrosis progresses, it can severely impair oral functions, such as eating, speaking, and swallowing. Moreover, 1.5-15% of OSF may eventually develop into oral squamous cell carcinoma (OSCC) (Shih et al. 2019). Currently, the treatment of OSF can only relieve its symptoms, but not cured it (Shih et al. 2019). Therefore, it is urgent to find a potent therapy for OSF to reverse or even block its progression and malignant transformation.

Numerous studies have shown that cellular senescence is closely related to fibrosis and cancer (Huang et al. 2021; Yao et al. 2021). Senescent cells exhibit cell cycle arrest and develop a secretory profile composed of growth factors, inflammatory cytokines, chemokines, and other bioactive molecules, termed the senescence-associated secretory phenotype (SASP) (Shmulevich & Krizhanovsky 2021). Cell cycle arrest prevents damaged cells from proliferating, and the secretion of SASP recruits immune cells to eliminate senescent cells, making cellular senescence a critical protective mechanism (Herranz & Gil 2018). Senescent cells, however, have a detrimental effect on neighboring cells by generating excessive SASP when they abnormally accumulate in tissues (Loo et al. 2020). For example, senescent alveolar type II cells contributed to lung fibrogenesis by activating the profibrotic phenotype of alveolar macrophages through secreting SASP (Rana et al. 2020). Through SASP, senescent hepatic stellate cells enhanced hepatocellular carcinoma cell growth and accelerated xenograft tumor growth (Li et al. 2020). Besides, senotherapy, which targets senescent cells, has been demonstrated that is an effective treatment for fibrosis and cancer (Amor et al. 2020). However, the mechanism of cellular senescence in OSF is still poorly understood.

Up to date, there has been relatively little study on cellular senescence in OSF. Rehman et al. reported in 2016 that senescent fibroblasts remodel the tissue microenvironment to promote the progression of OSF to OSCC through releasing SASP (Rehman et al. 2016). However, as the first barrier, far too little attention has been paid to the roles of the epithelium in the pathogenesis of OSF. Since epithelial atrophy is a characteristic pathological manifestation of OSF and OSCC originates from the epithelium, we speculated that epithelial cells of OSF may undergo premature senescence, which participates in OSF progression.

TGF-β1 is a multifunctional cytokine that plays a role in numerous physiological and pathological processes (Kim et al. 2018). In OSF, TGF-β1 is a major profibrotic factor, mainly by promoting fibroblast proliferation and transforming into myofibroblasts to produce extracellular matrix (Hsieh et al. 2018). Moreover, TGF-β1 may also play an important role in the tumorigenesis of OSF, as it has been shown to regulate epithelial-mesenchymal transition, immunosuppression, and stemness (Cave et al. 2020; Yeh et al. 2018). Gao et al. reported in 1997 that the mRNA level of TGF-β1 was the highest expressed in OSF epithelial tissue compared to the healthy mucosal tissue and oral lichen planus (Gao et al. 1997). In addition, our previous study also confirmed that TGF-β1 was predominantly expressed

89   in OSF epithelium, which was significantly higher than that in healthy mucosal epithelium (Wang et

90   al. 2018). These studies suggested that OSF epithelium is a major source of TGF-β1, which may be involved

91   in the fibrotic progression and carcinomagenesis of OSF by secreting excessive TGF-β1. However, it

92   remains unclear what pathological changes occur in OSF epithelium that causes the excessive

93   secretion of TGF-β1. We hope this study will contribute to the exploration of targeted therapy for OSF.

94   In this study, we demonstrated that OSF epithelial cells undergo premature senescence and could

95   play roles in OSF progression.

96

97   **2.   Materials and methods**

98   **2.1 Patient samples**

99   A total of 30 samples were collected from the center of stomatology, Xiangya Hospital from
100 September 2019 to May 2020. 21 OSF tissues were obtained from OSF patients without OSF therapy.
101 9 healthy oral mucosa (NOM) samples were obtained from healthy volunteers during surgical
102 removal of the lower third molars. All samples were diagnosed by pathological examination based on
103 the 2005 World Health Organization classification system. All research subjects gave written informed
104 consent in accordance with the Helsinki Declaration. This study was approved by the Medical Ethics
105 Committee of Xiangya Hospital, Central South University (ethics approval number 201803795).

106

107 **2.2 Immunohistochemistry assay**

108 The immunohistochemistry was performed as described previously (Min et al. 2020). Tissues
109 were fixed with 4% paraformaldehyde for 24h, and then were dehydrated in graded alcohol solutions
110 and embedded in paraffin. The paraffin-embedded tissues were sliced into 5-μm sections. The
111 following primary antibodies were used in immunohistochemistry: p16 (1:500, ab108349, Abcam), p21
112 (1:50, 2947T, Cell signaling technology, CST), alpha-smooth actin (α-SMA) (1:200, ab5694, Abcam),
113 proliferating cell nuclear antigen (PCNA) (1:16000, 2586S, CST). Phosphate-buffered saline (PBS) was
114 used instead of the primary antibody as a negative control, and NOM tissues were used as a positive
115 control. All slides were observed by microscopy (Leica Microsystems, Cambridge, UK). The staining
116 results were quantitatively evaluated using the Image-Pro-Plus 5.0 software to measure the mean
117 optical density (MOD) of positive p16, p21, PCNA, and α-SMA in OSF tissues (MOD = integral optical
118 density (IOD)/area of interest) (Hu et al. 2021). The epithelium or subepithelial areas of NOM and OSF
119 tissues were marked as the interest areas for analysis.

120

121 **2.3 Sudan black B staining**

122 To detect lipofuscin accumulation in OSF epithelium, Sudan black B solution was used to stain
123 the lipofuscin. Sudan black B staining (S109070, Aladdin) was carried out as described previously
124 (Georgakopoulou et al. 2013).

125

126 **2.4 Cell culture**

127 Human Oral Keratinocytes (HOKs) is currently the only normal oral epithelial cell line available,
128 which were cultured in complete Alpha MEM (10% FBS and 1% penicillin-streptomycin added) at
129 37℃, 5% CO_2 incubator (Wang et al. 2018). As the major components of betel nut, we used arecoline
130 to induce HOKs senescence. The half-maximal inhibitory concentrations (IC50) of arecoline in HOKs
131 were 200 μg/ml within 24h and 160 μg/ml within 48h by CCK8 assay, and then arecoline
132 concentrations were grouped accordingly. HOKs were randomly divided into 6 groups, and after
133 starvation in serum-free medium overnight, they were incubated with complete medium containing
134 different concentrations of arecoline (0, 20, 40, 80, 160, and 320 μg/ml) for 24h. Then, all groups were
135 replaced with complete medium, and the medium was changed every 3 days for 10-14 days.

136

137 **2.5 Senescence-associated β galactosidase (SA-β-gal) activity assay**

138   The SA-β-gal activity was performed using a SA-β-gal staining Kit (CS0030, Sigma-Aldrich)
139   following the manufacturer's instructions. Briefly, after senescence induction, HOKs were seeded into
140   24-well culture plates at a density of 1×10^4 cells per well. The next day, the cells were washed three
141   times with PBS and fixed by cell fixative solution in the SA-β-gal staining Kit for 7 min at room
142   temperature. Then, the cells were washed three times with PBS to remove the solution. The staining
143   mixture containing X-gal prepared following the instruction was incubated with the cells in a regular
144   incubator at 37℃ overnight without CO_2. The cells were observed by microscopy (Leica Microsystems,
145   Cambridge, UK). A total of 5 fields in each group were selected under the microscope and the total
146   cells and SA-β-gal positive cells in each field were counted by ImageJ 5.0. The proportion of SA-β-gal
147   positive cells was obtained by calculating the ratio of the average SA-β-gal positive cell number to the
148   average total cell number in each group.
149
150   **2.6 Immunofluorescence assay**
151   Immunofluorescence was applied to examine the expression of phosphor-histone H2A.X
152   (γH2A.X) in HOKs treated with different concentrations of arecoline. After senescence induction, the
153   cells were seeded into 24-wells culture plates at 1×10^4 per well density. The next day, the cells were
154   fixed with 4% paraformaldehyde for 10 min. Subsequently, the cells were permeabilized with 0.1%
155   Triton X-100 solution and blocked with 10% goat serum (ZLI-9056, ZSGB-BIO). After PBS washing,
156   the cells were incubated with monoclonal rabbit anti-γH2A.X primary antibody (1:400, 9718, CST) at
157   4℃ overnight. The next day, the cells were incubated with cy3-conjugated secondary antibody
158   (AP132C, Sigma) for 1 h in dark, and then counterstained with 4',6-Diamidino-2-phenylindole (C1002,
159   Beyotime) at room temperature for 1 min. Immunofluorescence images were acquired using a
160   fluorescence microscope (Leica Microsystems, Cambridge, UK). A total of 5 fields in each group were
161   selected under the microscope and the total cells and γH2A.X positive cells in each field were counted
162   by ImageJ 5.0. The proportion of γH2A.X positive cells was obtained by calculating the ratio of the
163   average γH2A.X positive cell number to the average total cell number in each group.
164
165   **2.7 Cell proliferation assay**
166   Cell proliferation ability was assessed by Cell Counting Kit 8 (CCK8) (A311-01, Vazyme). CCK8
167   assay was performed by the manufacturer's protocol. After senescence induction, HOKs were seeded
168   into 96-well plates at a density of 5000 cells per well and continually cultured for 0, 24, 48, 72, and 96
169   h. Then, CCK8 solution (10 μl) was added to each well for 2 h incubation at 37℃. The plates were
170   detected at the indicated time (0, 24, 48, 72, and 96 h) using a microplate reader (Synergy 2, Biotek) at
171   a wavelength of 450 nm.
172
173   **2.8 Quantitative reverse transcription polymerase chain reaction (qRT-PCR) assay**
174   Total RNA was extracted from HOKs treated with different concentrations of arecoline using
175   TRIzol reagent (15596026, Invitrogen). The total RNA was reverse transcribed to cDNA using
176   RevertAid™ Master Mix, with DNase I Kit (M16325, Thermo Scientific) according to the
177   manufacturer's protocol. qPCR was performed using Maxima SYBR Green qPCR Master Mix (K0252,
178   Thermo Scientific) on a Real-Time PCR Detection System (CFX96, Bio-Rad) according to the

179 manufacturer's protocol. All qPCR primers were listed in Table 1. The relative mRNA expression was
180 calculated using the $2^{-\Delta\Delta Ct}$ method. GAPDH served as housekeeping gene. The value of negative
181 control group was used to calculate the relative fold change in expression value.

182

183 **2.9 Western blotting assay**

184 The total protein was extracted from HOKs treated with different concentrations of arecoline
185 using SDS lysis buffer (P0013G, Beyotime). The total protein concentration was detected using
186 Pierce™ BCA Protein Assay Kit (23225, Thermo Fisher Scientific). A total of 40 μg protein was added
187 to 10% polyacrylamide gel and transferred to polyvinylidene fluoride (PVDF) membranes. The
188 membranes were blocked with 5% skim milk for 1 hour at room temperature. After PBST washing
189 three times, the membranes were incubated with primary antibodies overnight at 4℃ overnight: p16
190 (1:2000, ab108349, Abcam), p21 (1:2000, 2946, CST), p53 (1:1000, 48818, CST), transforming growth
191 factor β1 (TGF-β1) (1:1000, ab215715, Abcam), and GAPDH (1:1000, 5174T, CST). Then, the
192 membranes were incubated with the corresponding horseradish peroxidase-conjugated secondary
193 antibodies (anti-Rabbit/mouse 1:5000~10000, SA00001-1/2, Proteintech) for 1 hour at room
194 temperature. The membranes were developed using SuperSignal™ West Pico PLUS
195 chemiluminescent substrate (34580, Thermo Fisher Scientific) and detected by a chemiluminescent
196 imaging system (MiniChemi 610, Sagecreation). and analyzed using the ImageJ 5.0 version software.

197

198 **2.10 Enzyme-linked immunosorbent (ELISA) assay**

199 Levels of TGF-β1 in supernatants were measured by the Human TGF-β1 Elisa Kit (PT880,
200 Beyotime) following the manufacturer's protocol. The absorbance of samples was detected at 450 nm
201 using a microplate reader (Synergy 2, Biotek). The TGF-β1 concentration of each sample was
202 determined based on a standard curve we prepared according to the manufacturer's protocol.

203

204 **2.11 Statistical analysis**

205 All experiments were conducted in triplicate and repeated at least 3 times. All data were shown
206 as mean ± standard deviation. Continuous variables were assessed by the student's t test or Mann-
207 Whitney U test according to the normality test. Spearman's correlation was used to analyze the
208 correlation. *P* value < 0.05 was considered statistically significant. Statistical analysis was performed
209 using SPSS 24.0 software.

210

211 **3. Results**

212 **3.1 The epithelium of OSF undergoes premature senescence**

213   p16 and p21 belong to cyclin-dependent kinase inhibitors, which are major drivers of the cycle
214 arrest in senescence and have been confirmed to be one of the defining features of senescent cells
215 (Calcinotto et al. 2019). Therefore, we detected the expressions of p16 and p21 in the epithelium of
216 OSF and healthy tissues. We found that p16 and p21 were overexpressed in OSF epithelium compared
217 with the healthy epithelium (Figure 1A-D). In contrast, PCNA, which indicates cellular proliferation,
218 was highly expressed in the epithelium of NOM (Figure 1A, B, E). Moreover, the expressions of p16
219 and p21 were negatively correlated with PCNA in OSF epithelial tissues (Figure 1H-K).

220   To further confirm epithelial cells senescence in OSF, we detected the accumulation of lipofuscin
221 in OSF epithelium by Sudan Black staining. Lipofuscin is abnormally accumulated in senescent cells,
222 another well-established senescence marker (Georgakopoulou et al. 2013). After Sudan black B
223 staining, we found that the lipofuscin was widely distributed in OSF epithelium (Figure 1G).

224

225 **3.2 Correlation between the epithelial cell senescence and myofibroblast activation in human OSF**
226 **tissues**

227   To further investigate the correlation between the epithelial cell senescence and myofibroblast
228 activation in OSF tissue, we detected the expression of α-SMA that is a characteristic marker of
229 myofibroblast activation. We observed that there were α-SMA positive spindle cells located in the
230 lamina propria adjacent to the epithelium of OSF (Figure 1B). In sharp contrast, we only detected rings
231 of α-SMA positive cells representing blood vessels in the lamina propria of healthy tissues (Figure
232 1A). We hardly found the α-SMA positive spindle cells in healthy tissues. Moreover, the expression
233 of α-SMA in OSF tissues was extremely higher than that in healthy tissues ($p < 0.001$, Figure 1F).
234 Further analysis revealed that α-SMA expression in OSF tissues was positively correlated with the
235 expressions of senescence markers, p21 and p16 ($p < 0.01$, Figure 1H).

236

237 **3.3 Arecoline induced senescence-like cell morphology and suppressed cell proliferation in HOKs**

238   Since OSF is an oral mucosal disease associated with the chewing of betel nut, we choose arecoline
239 to induce HOKs senescence due to it is a major component of betel nut. To confirm HOKs developing
240 senescence, we examined senescence-associated phenotypes in HOKs.

241   After HOKs were treated with different concentrations of arecoline for 24h, they gradually
242 appeared an enlarged and flattened morphology, following another 5-7 days of culture (Figure 2A).
243 Meanwhile, the enlarged and flattened HOKs also showed SA-β-gal positive staining (Figure 2A). The
244 proportion of SA-β-gal positive HOKs was gradually increased with arecoline concentration. Among
245 different concentrations of arecoline, the 320 μg/ml group had the highest proportion of SA-β-gal
246 positive HOKs compared with other groups ($p < 0.05$, Figure 2B). Moreover, the surface area of SA-β-
247 gal positive cells was about 10-fold more than that of SA-β-gal negative cells ($p < 0.05$, Figure 2C).
248 CCK8 assay showed that compared with that of other groups, the proliferation ability of the 320 μg/ml
249 group was largely suppressed after senescence induction ($p < 0.05$, Figure 2D).

250

251 **3.4 Arecoline induced DNA damage response (DDR) in HOKs**

252   The phosphorylated-histone H2A was detected in HOKs after senescence induction, a hallmark
253   of DNA double-strand breakage in cells, because DNA damage stimulates DNA damage response
254   (DDR) that triggers senescence (Di Micco et al. 2021; Gorgoulis et al. 2019). We found that γH2A.X
255   was mainly detected in HOKs treated with high concentrations of arecoline (160 and 320 µg/ml)
256   (Figure 3A). The proportion of γH2A.X positive HOKs was elevated with arecoline concentration, and
257   that in the 320 µg/ml group was significantly higher than in other groups ($p < 0.05$, Figure 3B).
258   Moreover, we observed that γH2A.X was mainly expressed in the nucleus of the enlarged and flatted
259   HOKs (Figure 3C).
260

261   **3.5 Arecoline-induced HOK senescence was associated with p53/p21 pathway**
262   Cell cycle arrest of senescent cells is controlled by activation of the p53/p21 or p16/Rb pathway
263   (Gorgoulis et al. 2019). Since most of HOKs in the 320 µg/ml group undergo senescence, we compared
264   the levels of p16, p21, and p53 between the groups of the negative control (0 µg/ml) and the 320 µg/ml.
265   We found that p21 expression was dramatically upregulated at the protein and mRNA level ($p < 0.01$,
266   Figure 4A, B), while p53 expression was on the rise only at the protein level in the 320 µg/ml group
267   ($p < 0.05$, Figure 4A, C). No difference was observed in p16 at protein and mRNA levels in both groups
268   (Figure 4A).
269

270   **3.6 The synthesis and secretion of TGF-β1 are increased in senescent HOKs**
271   Growth factors are a prominent constituent of SASP. Given that TGF-β1 is a well-known
272   profibrotic factor, we examined the protein and mRNA levels of TGF-β1 between the groups of the
273   negative control (0 µg/ml) and the 320 µg/ml. The protein and mRNA levels of TGF-β1 in the 320 µg/ml
274   group were all significantly upregulated, compared with the negative control group ($p < 0.05$, Figure
275   4D). In addition, although the density of HOKs in the 320 µg/ml group after senescence induction was
276   approximately 30-40% of that in the negative control group, we found that the levels of TGF-β1 in the
277   supernatant of the 320 µg/ml group were increased approximately 2-fold compared to the control
278   group ($p < 0.01$, Figure 4E).

Discussion

280

281   The treatments of OSF are currently used to effectively control symptoms and improve oral

282 functions and the life quality of OSF patients (Shih et al. 2019). Yet these treatments can neither

283 completely cure OSF nor block its transformation to OSCC. Recently, senescent cells have been shown

284 to participate in the development of fibrotic diseases and tumors (Huang et al. 2021; Yao et al. 2021),

285 and were regarded as a novel target for effectively suppressing the disease progression (Amor et al.

286 2020). In OSF, the cellular senescence of fibroblasts has received the first attention. It has been

287 confirmed that fibroblasts can undergo senescence under adverse stimuli and participate in the

288 process of fibrosis and malignant transformation of OSF (Pitiyage et al. 2011; Rehman et al. 2016).

289 However, as a direct target of adverse stimuli, OSF epithelium has not received much attention.

290 Currently, there was a speculation that the cause of epithelial atrophy in OSF may be epithelial cell

291 senescence, whereas the senescence escape will make them susceptible to malignant transformation

292 (Sharma et al. 2021). To our knowledge, our work is the first to focus on cellular senescence in the

293 epithelium of OSF patients.

294   In the present study, we found that lipofuscin was abnormally increased in OSF epithelium.

295 Additionally, the expressions of p16 and p21 were elevated in the epithelium of OSF by

296 immunohistochemistry assay. Their expressions were negatively correlated to PCNA expression,

297 which was hardly expressed in the epithelium of OSF. Both p16 and p21 are well-established markers

298 of cellular senescence and belong to the Cyclin-Dependent Kinase Inhibitor family, mediating cell

299 cycle arrest to suppress cell proliferation (Gorgoulis et al. 2019). These results provided evidence that

300 OSF epithelium undergoes cellular senescence, which results in epithelial atrophy. Meanwhile, we

301 also found that p16 and p21 expression were positively correlated with α-SMA expression, a marker

302 of the activated myofibroblast. Activated myofibroblasts are the major source of collagen in fibrosis

303 (Lee et al. 2021). These results indicated that the epithelial senescence was associated with the

304 myofibroblast activation. Tian et al. have confirmed that senescent alveolar epithelial cells activated

305 myofibroblasts through intercellular communication in lung fibrosis (Tian et al. 2019). These findings

306 implied that senescent epithelial cells could activate myofibroblasts by intercellular communication.

307 Therefore, to further investigate the roles of senescent epithelial cells, we used arecoline to induce

308 HOKs senescence in vitro, as HOKs are immortalized epithelial cells obtained from the basal layer of

309 oral mucosa tissues.

310   Arecoline has been shown to generate reactive oxygen species (ROS) in different types of cells

311 (Shih et al. 2020; Shih et al. 2021), and ROS is one of the common triggers of cellular senescence (Di

312 Micco et al. 2021). We found that HOKs exhibited various senescence-associated phenotypes under

313 the short-duration stimulation of arecoline. The proportion of these cells showed a dose-dependent

314 relationship with arecoline. A possible explanation for this might be that arecoline raised intracellular

315 reactive oxygen species (ROS) levels in a dose-dependent manner (Yen et al. 2011). Moreover, γH2A.X

316 foci localized in the nucleus of senescent-like cells, and the expressions of p53 and p21 were obviously

317 higher in HOKs treated with 320 μg/ml arecoline than in HOKs without arecoline. The formation of

318 γH2A.X foci represents the activation of DNA damage response (DDR) and dysregulation of the cell

319 cycle (Hernandez-Segura et al. 2018). The DDR can activate the p53/p21 pathway, and p21 is

320 responsible for initiating senescence (Di Micco et al. 2021). These findings presented that arecoline can

321   induce HOKs senescence, which is consistent with the study of Patil et al. (Patil et al. 2021). However,
322   our study also provided an insight that arecoline-induced senescence in HOKs is closely linked to the
323   p53/p21 pathway. In addition, TGF-β1 expressions were significantly increased at protein and mRNA
324   levels in HOKs treated with 320 μg/ml arecoline, compared with HOKs without arecoline. These
325   results indicated that senescent HOKs can synthesize more TGF-β1. Although TGF-β1 is one of the
326   common components of SASP, the composition of SASP depends on cell type and stimulus.
327   Subsequently, we examined TGF-β1 levels in the supernatant to determine that senescent HOKs can
328   secrete excessive TGF-β1.
329   As identified in ELISA experiments, we found that secreted TGF-β1 levels in senescent HOK
330   supernatants were approximately 2-fold higher than in negative control samples. These results
331   suggested that senescent HOKs could release excessive TGF-β1. Our previous study reported that
332   TGF-β1 was overexpressed in the epithelium of OSF (Wang et al. 2018). Consequently, senescent
333   epithelial cells could be one of the major cellular sources of upregulated TGF-β1 expression in the
334   epithelium of OSF samples.
335   As a pleiotropic cytokine, firstly, TGF-β1 has been demonstrated to induce myofibroblasts
336   differentiation to facilitate fibrosis (Huang et al. 2020; Little et al. 2020; Zhang et al. 2021), and
337   secondly, TGF-β1 can participate in tumorigenesis by mediating epithelial-mesenchymal transition,
338   immunosuppression, and stemness (Cave et al. 2020; Yeh et al. 2018). Moreover, TGF-β1 has also been
339   shown to have a pro-senescence effect, which can induce myofibroblasts senescence through
340   autophagy deregulation or TGF-β-dependent mechanisms (Hassona et al. 2013; Tan et al. 2021).
341   Hence, it raises the possibility that there may be a paracrine positive-feedback loop to amplify
342   senescence and reinforce TGF-β1 signaling in OSF epithelium (Figure 5).
343   Accordingly, targeting the senescent epithelial cells may constitute a promising therapeutic
344   approach for OSF. Amor et al. recently reported that chimeric antigen receptor T cells can effectively
345   eliminate senescent cells, which extend the lifespan of mice harboring lung adenocarcinoma and
346   restore tissue homeostasis in mice with liver fibrosis (Amor et al. 2020).
347   In summary, we found that the epithelium of OSF undergoes premature senescence, and there is
348   a positive correlation between senescent epithelial cells and myofibroblasts activation. In addition,
349   our study indicated that senescent HOKs secrete excessive TGF-β1, which suggested that senescent
350   epithelial cells could affect surrounding cells by TGF-β1 secretion. Moreover, this research has an
351   important implication for developing targeted therapeutics for senescent epithelial cells in OSF, which
352   may be beneficial for reversing and blocking its progression and malignant transformation.
353
Conclusions
355   Our study first revealed that cellular senescence occurs in OSF epithelium, and senescent
356   epithelial cells are an important source of TGF-β1 in OSF epithelium. These results provide a new
357   perspective for OSF target therapy against senescent epithelium.
358

359 **Conflict of interest**

360 We have no conflicts of interest.

361

362 **Acknowledgements**

363 We thank Professor Sun Zhijun in Hospital of Stomatology Wuhan University for supporting HOKs.

364

365 **Reference**

366 **Amor C, Feucht J, Leibold J, Ho YJ, Zhu C, Alonso-Curbelo D, Mansilla-Soto J, Boyer JA, Li X, Giavridis**

367 **T, Kulick A, Houlihan S, Peerschke E, Friedman SL, Ponomarev V, Piersigilli A, Sadelain M,**

368 **and Lowe SW. 2020.** Senolytic CAR T cells reverse senescence-associated pathologies. Nature

369 583:127-132 DOI 10.1038/s41586-020-2403-9.

370 **Angadi PV, and Rekha KP. 2011.** Oral submucous fibrosis: a clinicopathologic review of 205 cases in

371 Indians. Oral Maxillofac Surg 15:15-19 DOI 10.1007/s10006-010-0225-x.

372 **Calcinotto A, Kohli J, Zagato E, Pellegrini L, Demaria M, and Alimonti A. 2019.** Cellular Senescence:

373 Aging, Cancer, and Injury. Physiol Rev 99:1047-1078 DOI 10.1152/physrev.00020.2018.

374 **Cave DD, Di Guida M, Costa V, Sevillano M, Ferrante L, Heeschen C, Corona M, Cucciardi A, and**

375 **Lonardo E. 2020.** TGF-β1 secreted by pancreatic stellate cells promotes stemness and

376 tumourigenicity in pancreatic cancer cells through L1CAM downregulation. Oncogene 39:4271-

377 4285 DOI 10.1038/s41388-020-1289-1.

378 **Di Micco R, Krizhanovsky V, Baker D, and d'Adda di Fagagna F. 2021.** Cellular senescence in ageing:

379 from mechanisms to therapeutic opportunities. Nat Rev Mol Cell Biol 22:75-95 DOI 10.1038/s41580-

380 020-00314-w.

381 **Gao Y, Ling T, and Wu H. 1997.** Expression of transforming growth factor beta 1 in keratinocytes of oral

382 submucous fibrosis tissue. Zhonghua Kou Qiang Yi Xue Za Zhi 32:239-241.

383 **Georgakopoulou EA, Tsimaratou K, Evangelou K, Fernandez Marcos PJ, Zoumpourlis V, Trougakos IP,**

384 **Kletsas D, Bartek J, Serrano M, and Gorgoulis VG. 2013.** Specific lipofuscin staining as a novel

385 biomarker to detect replicative and stress-induced senescence. A method applicable in cryo-

386 preserved and archival tissues. Aging (Albany NY) 5:37-50 DOI 10.18632/aging.100527.

387 **Gorgoulis V, Adams PD, Alimonti A, Bennett DC, Bischof O, Bishop C, Campisi J, Collado M,**

388 **Evangelou K, Ferbeyre G, Gil J, Hara E, Krizhanovsky V, Jurk D, Maier AB, Narita M,**

389 **Niedernhofer L, Passos JF, Robbins PD, Schmitt CA, Sedivy J, Vougas K, von Zglinicki T, Zhou**

390 **D, Serrano M, and Demaria M. 2019.** Cellular Senescence: Defining a Path Forward. Cell 179:813-

391 827 DOI 10.1016/j.cell.2019.10.005.

392 **Hassona Y, Cirillo N, Lim KP, Herman A, Mellone M, Thomas GJ, Pitiyage GN, Parkinson EK, and**

393 **Prime SS. 2013.** Progression of genotype-specific oral cancer leads to senescence of cancer-

394 associated fibroblasts and is mediated by oxidative stress and TGF-β. Carcinogenesis 34:1286-1295

395 DOI 10.1093/carcin/bgt035.

396 **Hernandez-Segura A, Nehme J, and Demaria M. 2018.** Hallmarks of Cellular Senescence. Trends Cell Biol

397 28:436-453 DOI 10.1016/j.tcb.2018.02.001.

398 **Herranz N, and Gil J. 2018.** Mechanisms and functions of cellular senescence. J Clin Invest 128:1238-1246

399 DOI 10.1172/jci95148.

400 **Hsieh YP, Wu KJ, Chen HM, and Deng YT. 2018.** Arecoline activates latent transforming growth factor β1

401 via mitochondrial reactive oxygen species in buccal fibroblasts: Suppression by epigallocatechin-

402 3-gallate. J Formos Med Assoc 117:527-534 DOI 10.1016/j.jfma.2017.07.003.

403 **Hu X, Xia K, Xiong H, and Su T. 2021.** G3BP1 may serve as a potential biomarker of proliferation, apoptosis,

404 and prognosis in oral squamous cell carcinoma. J Oral Pathol Med 50:995-1004 DOI

405 10.1111/jop.13199.

406 **Huang Y, Xie Y, Abel PW, Wei P, Plowman J, Toews ML, Strah H, Siddique A, Bailey KL, and Tu Y.**
407   **2020.** TGF-β1-induced miR-424 promotes pulmonary myofibroblast differentiation by targeting
408   Slit2 protein expression. Biochem Pharmacol 180:114172 DOI 10.1016/j.bcp.2020.114172.

409 **Huang Y, Yang X, Meng Y, Shao C, Liao J, Li F, Li R, Jing Y, and Huang A. 2021.** The hepatic senescence-
410   associated secretory phenotype promotes hepatocarcinogenesis through Bcl3-dependent
411   activation of macrophages. Cell Biosci 11:173 DOI 10.1186/s13578-021-00683-5.

412 **Kim KK, Sheppard D, and Chapman HA. 2018.** TGF-β1 Signaling and Tissue Fibrosis. Cold Spring Harb
413   Perspect Biol 10(4):a022293 DOI 10. 10.1101/cshperspect.a022293.

414 **Lee YH, Liao YW, Lu MY, Hsieh PL, and Yu CC. 2021.** LINC00084/miR-204/ZEB1 Axis Mediates
415   Myofibroblastic Differentiation Activity in Fibrotic Buccal Mucosa Fibroblasts: Therapeutic Target
416   for Oral Submucous Fibrosis. J Pers Med 11:707 DOI 10.3390/jpm11080707.

417 **Li F, Huangyang P, Burrows M, Guo K, Riscal R, Godfrey J, Lee KE, Lin N, Lee P, Blair IA, Keith B, Li**
418   **B, and Simon MC. 2020.** FBP1 loss disrupts liver metabolism and promotes tumorigenesis through
419   a hepatic stellate cell senescence secretome. Nat Cell Biol 22:728-739 DOI 10.1038/s41556-020-0511-
420   2.

421 **Little K, Llorián-Salvador M, Tang M, Du X, Marry S, Chen M, and Xu H. 2020.** Macrophage to
422   myofibroblast transition contributes to subretinal fibrosis secondary to neovascular age-related
423   macular degeneration. J Neuroinflammation 17:355 DOI 10.1186/s12974-020-02033-7.

424 **Loo TM, Miyata K, Tanaka Y, and Takahashi A. 2020.** Cellular senescence and senescence-associated
425   secretory phenotype via the cGAS-STING signaling pathway in cancer. Cancer Sci 111:304-311 DOI
426   10.1111/cas.14266.

427 **Min A, Xiong H, Wang W, Hu X, Wang C, Mao T, Yang L, Huang D, Xia K, and Su T. 2020.** CD147
428   promotes proliferation and migration of oral cancer cells by inhibiting junctions between E-
429   cadherin and β-catenin. J Oral Pathol Med 49:1019-1029 DOI 10.1111/jop.13088.

430 **Patil S, Sarode SC, Ashi H, Ali Baeshen H, Thirumal Raj A, Awan KH, Gondivkar S, Ramchandra**
431   **Gadbail A, and Sarode GS. 2021.** Triphala extract negates arecoline-induced senescence in oral
432   mucosal epithelial cells in vitro. Saudi J Biol Sci 28:2223-2228 DOI 10.1016/j.sjbs.2021.01.011.

433 **Pitiyage GN, Slijepcevic P, Gabrani A, Chianea YG, Lim KP, Prime SS, Tilakaratne WM, Fortune F, and**
434   **Parkinson EK. 2011.** Senescent mesenchymal cells accumulate in human fibrosis by a telomere-
435   independent mechanism and ameliorate fibrosis through matrix metalloproteinases. J Pathol
436   223:604-617 DOI 10.1002/path.2839.

437 **Rana T, Jiang C, Liu G, Miyata T, Antony V, Thannickal VJ, and Liu RM. 2020.** PAI-1 Regulation of TGF-
438   β1-induced Alveolar Type II Cell Senescence, SASP Secretion, and SASP-mediated Activation of
439   Alveolar Macrophages. Am J Respir Cell Mol Biol 62:319-330 DOI 10.1165/rcmb.2019-0071OC.

440 **Rehman A, Ali S, Lone MA, Atif M, Hassona Y, Prime SS, Pitiyage GN, James EL, and Parkinson EK.**
441   **2016.** Areca nut alkaloids induce irreparable DNA damage and senescence in fibroblasts and may
442   create a favourable environment for tumour progression. J Oral Pathol Med 45:365-372 DOI
443   10.1111/jop.12370.

444 **Sharma M, Hunter KD, Fonseca FP, and Radhakrishnan R. 2021.** Emerging role of cellular senescence in
445   the pathogenesis of oral submucous fibrosis and its malignant transformation. Head Neck 43:3153-
446   3164 DOI 10.1002/hed.26805.

447 **Shih LJ, Wang JY, Jheng JY, Siao AC, Lin YY, Tsuei YW, Kuo YC, Chuu CP, and Kao YH. 2020.** Betel Nut
448   Arecoline Induces Different Phases of Growth Arrest between Normal and Cancerous Prostate
449   Cells through the Reactive Oxygen Species Pathway. Int J Mol Sci 21:9219 DOI
450   10.3390/ijms21239219.
451 **Shih YH, Chiu KC, Wang TH, Lan WC, Tsai BH, Wu LJ, Hsia SM, and Shieh TM. 2021.** Effects of
452   melatonin to arecoline-induced reactive oxygen species production and DNA damage in oral
453   squamous cell carcinoma. J Formos Med Assoc 120:668-678 DOI 10.1016/j.jfma.2020.07.037.
454 **Shih YH, Wang TH, Shieh TM, and Tseng YH. 2019.** Oral Submucous Fibrosis: A Review on
455   Etiopathogenesis, Diagnosis, and Therapy. Int J Mol Sci 20:2940 DOI 10.3390/ijms20122940.
456 **Shmulevich R, and Krizhanovsky V. 2021.** Cell Senescence, DNA Damage, and Metabolism. Antioxid
457   Redox Signal 34:324-334 DOI 10.1089/ars.2020.8043.
458 **Tan ML, Parkinson EK, Yap LF, and Paterson IC. 2021.** Autophagy is deregulated in cancer-associated
459   fibroblasts from oral cancer and is stimulated during the induction of fibroblast senescence by TGF-
460   β1. Sci Rep 11:584 DOI 10.1038/s41598-020-79789-8.
461 **Tian Y, Li H, Qiu T, Dai J, Zhang Y, Chen J, and Cai H. 2019.** Loss of PTEN induces lung fibrosis via
462   alveolar epithelial cell senescence depending on NF-κB activation. Aging Cell 18:e12858 DOI
463   10.1111/acel.12858.
464 **Tilakaratne WM, Klinikowski MF, Saku T, Peters TJ, and Warnakulasuriya S. 2006.** Oral submucous
465   fibrosis: review on aetiology and pathogenesis. Oral Oncol 42:561-568 DOI
466   10.1016/j.oraloncology.2005.08.005.
467 **Wang W, Xiong H, Hu Z, Zhao R, Hu Y, Chen W, Han Y, Yang L, Hu X, Wang C, Mao T, Xia K, and Su
468   T. 2018.** Experimental study on TGF-β1-mediated CD147 expression in oral submucous fibrosis.
469   Oral Dis 24:993-1000 DOI 10.1111/odi.12845.
470 **Yang HW, Yu CC, Hsieh PL, Liao YW, Chu PM, Yu CH, and Fang CY. 2021.** Arecoline enhances miR-21
471   to promote buccal mucosal fibroblasts activation. J Formos Med Assoc 120:1108-1113 DOI
472   10.1016/j.jfma.2020.10.019.
473 **Yao C, Guan X, Carraro G, Parimon T, Liu X, Huang G, Mulay A, Soukiasian HJ, David G, Weigt SS,
474   Belperio JA, Chen P, Jiang D, Noble PW, and Stripp BR. 2021.** Senescence of Alveolar Type 2
475   Cells Drives Progressive Pulmonary Fibrosis. Am J Respir Crit Care Med 203:707-717 DOI
476   10.1164/rccm.202004-1274OC.
477 **Yeh HW, Hsu EC, Lee SS, Lang YD, Lin YC, Chang CY, Lee SY, Gu DL, Shih JH, Ho CM, Chen CF, Chen
478   CT, Tu PH, Cheng CF, Chen RH, Yang RB, and Jou YS. 2018.** PSPC1 mediates TGF-β1 autocrine
479   signalling and Smad2/3 target switching to promote EMT, stemness and metastasis. Nat Cell Biol
480   20:479-491 DOI 10.1038/s41556-018-0062-y.
481 **Yen CY, Lin MH, Liu SY, Chiang WF, Hsieh WF, Cheng YC, Hsu KC, and Liu YC. 2011.** Arecoline-
482   mediated inhibition of AMP-activated protein kinase through reactive oxygen species is required
483   for apoptosis induction. Oral Oncol 47:345-351 DOI 10.1016/j.oraloncology.2011.02.014.
484 **Zhang B, Gao L, Shao C, Deng M, and Chen L. 2021.** Arecoline Enhances Phosphodiesterase 4A Activity
485   to Promote Transforming Growth Factor-β-Induced Buccal Mucosal Fibroblast Activation via
486   cAMP-Epac1 Signaling Pathway. Front Pharmacol 12:722040 DOI 10.3389/fphar.2021.722040.
487

488

489 **Figure Legends:**

490 **Figure 1. The expressions and correlation of p16, p21, PCNA, and α-SMA in healthy oral mucosa**

491 **(NOM) and oral submucous fibrosis (OSF). A-B** The representative images of p16, p21, PCNA, and

492 α-SMA expressions detected by immunohistochemistry (IHC) in NOM and OSF tissues. **C-F**

493 Quantification of the expressions of p16, p21, PCNA, and α-SMA in NOM and OSF tissues. **G** The

494 representative images of lipofuscin expression detected by Sudan Black B staining in the epithelial of

495 NOM and OSF tissues (black arrow). **H** The correlation between p16 and α-SMA expressions in

496 NOM and OSF tissues. **I** The correlation between p16 and PCNA expressions in NOM and OSF

497 tissues. **J** The correlation between p21 and α-SMA expressions in NOM and OSF tissues. **K** The

498 correlation between p21 and PCNA expressions in NOM and OSF tissues. *$p < 0.05$, **$p < 0.01$, ***$p <$

499 0.001, and ****$p < 0.0001$. Scale bar: 100μm in 100×, 25μm in 400×.

500

501 **Figure 2. The performance of senescence-associated beta galactosidase (SA-β-gal) staining, cell**

502 **morphology, and cell proliferation in human oral keratinocytes (HOKs) after senescence**

503 **induction. A** The representative images of SA-β-gal staining and cell morphology in HOKs treated

504 with different concentrations of arecoline (SA-β-gal positive cell: black arrow, green). **B** The

505 proportion of SA-β-gal positive cells in HOKs treated with different concentrations of arecoline. **C**

506 Quantification of the surface area of SA-β-gal negative HOKs and SA-β-gal positive HOKs (SA-β-gal

507 negative HOK: black arrow, SA-β-gal positive HOK: white arrow). **D** The cell proliferation of HOKs

508 treated with different concentrations of arecoline. *$p < 0.05$, ** $p < 0.01$, *** $p < 0.001$, **** $p < 0.0001$.

509 Scale bar: 100μm in 100×.

510

511 **Figure 3. The expression of phosphor-histone H2A.X (γH2A.X) in HOKs treated with different**

512 **concentrations of arecoline after senescence induction. A** The representative images of γH2A.X

513 expression in HOKs treated with the different concentrations of arecoline (blue: DAPI, red: γH2A.X,

514 γH2A.X positive cell: white arrow). **B** The proportion of γH2A.X positive cells in HOKs treated with

515 differentiation concentrations of arecoline. **C** The representative images of the senescent HOK (blue:

516 DAPI, red: γH2A.X). *$p < 0.05$, ** $p < 0.01$, *** $p < 0.001$, **** $p < 0.0001$. Scale bar: 100μm in 100×, 50μm

517 in 200×.

518

519 **Figure 4. The expressions of p16, p21, p53, and TGF-β1 in HOKs treated with 0μg/ml arecoline or**

520 **320 μg/ml arecoline after senescence induction. A** The representative images of p16, p21, p53, TGF-

521 β1, and GAPDH protein levels in HOKs treated with 0 μg/ml or 320 μg/ml arecoline. **B**

522 Quantification expressions of p21 at protein and mRNA levels in HOKs treated with 0 μg/ml or 320

523 μg/ml arecoline. **C** Quantification expressions of p53 at protein and mRNA levels in HOKs treated

524 with 0 μg/ml or 320 μg/ml arecoline. **D** Quantification expressions of TGF-β1 at protein and mRNA

525 levels in HOKs treated with 0 μg/ml or 320 μg/ml arecoline. **E** TGF-β1 expression in supernatants of

526 HOKs treated with 0 μg/ml or 320 μg/ml arecoline. *$p < 0.05$, ** $p < 0.01$, *** $p < 0.001$, **** $p < 0.0001$.

527

528 **Figure 5. The mechanism diagram for the role of senescent epithelial cells in the development of**

529 **OSF.**

530

Figure 1

The expressions and correlation of p16, p21, PCNA, and α-SMA in normal oral mucosa (NOM) and oral submucous fibrosis (OSF).

A-B The representative images of p16, p21, PCNA, and α-SMA expressions detected by immunohistochemistry (IHC) in NOM and OSF tissues. **C-F** Quantification of the expressions of p16, p21, PCNA, and α-SMA in NOM and OSF tissues. **G** The representative images of lipofuscin expression detected by Sudan Black B staining in the epithelial of NOM and OSF tissues (black arrow). **H** The correlation between p16 and α-SMA expressions in NOM and OSF tissues. **I** The correlation between p16 and PCNA expressions in NOM and OSF tissues. **J** The correlation between p21 and α-SMA expressions in NOM and OSF tissues. **K** The correlation between p21 and PCNA expressions in NOM and OSF tissues. $*p < 0.05$, $**p < 0.01$, $***p < 0.001$, and $****p < 0.0001$. Scale bar: 100μm in 100×, 25μm in 400×.
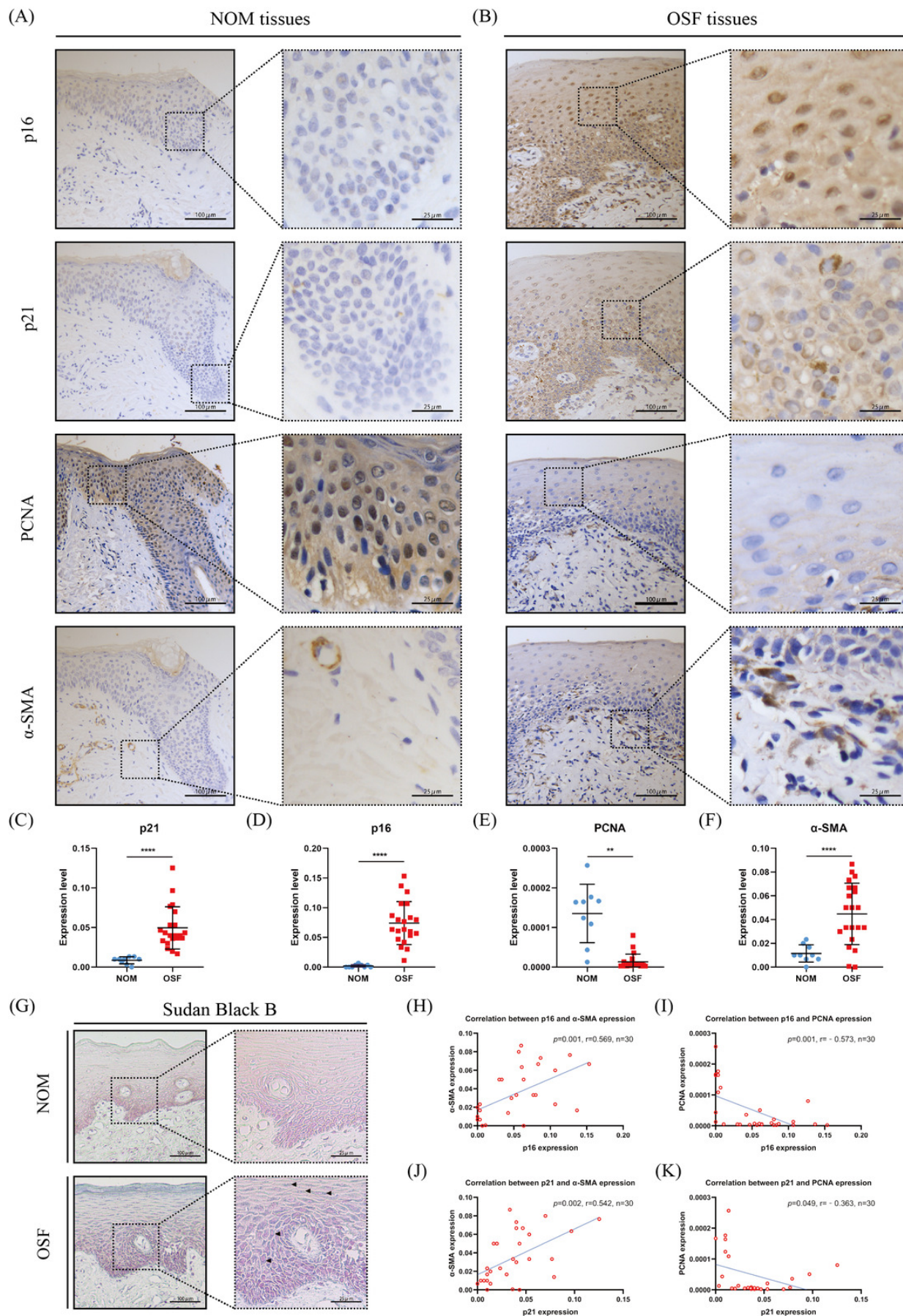
(A) NOM tissues

(B) OSF tissues

p16

p21

PCNA

α-SMA

(C) p21

(D) p16

(E) PCNA

(F) α-SMA

(G) Sudan Black B

NOM

OSF

(H) Correlation between p16 and α-SMA epression
p=0.001, r=0.569, n=30

(I) Correlation between p16 and PCNA epression
p=0.001, r= - 0.573, n=30

(J) Correlation between p21 and α-SMA epression
p=0.002, r=0.542, n=30

(K) Correlation between p21 and PCNA epression
p=0.049, r= - 0.363, n=30

Figure 2

The performance of senescence-associated beta galactosidase (SA-β-gal) staining, cell morphology, and cell proliferation in human oral keratinocytes (HOKs) after senescence induction.

A The representative images of SA-β-gal staining and cell morphology in HOKs treated with different concentrations of arecoline (SA-β-gal positive cell: black arrow, green). **B** The proportion of SA-β-gal positive cells in HOKs treated with different concentrations of arecoline. **C** Quantification of the surface area of SA-β-gal negative HOKs and SA-β-gal positive HOKs (SA-β-gal negative HOK: black arrow, SA-β-gal positive HOK: white arrow). **D** The cell proliferation of HOKs treated with different concentrations of arecoline. *$p < 0.05$, ** $p < 0.01$, *** $p < 0.001$, **** $p < 0.0001$. Scale bar: 100μm in 100×.

(A)
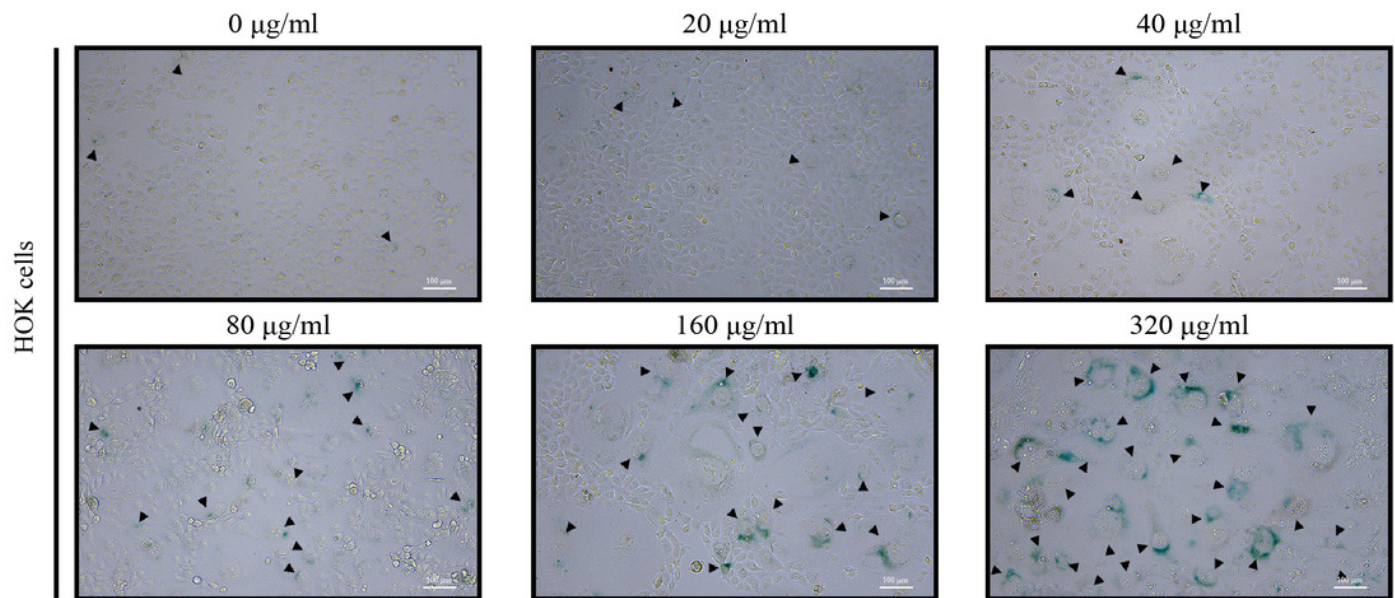
(B)
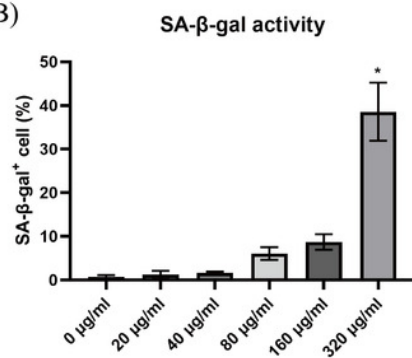
(C)
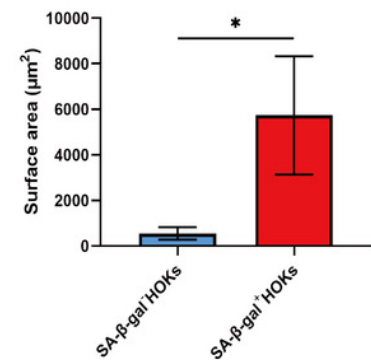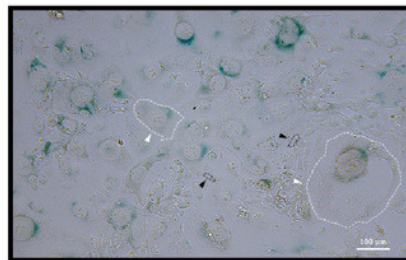
(D)
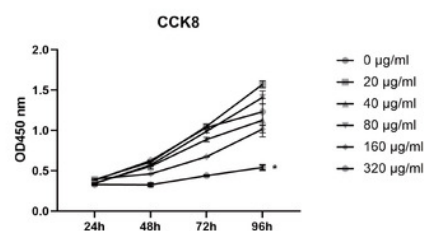
Figure 3

The expression of phosphor-histone H2A.X (γH2A.X) in HOKs treated with different concentrations of arecoline after senescence induction.

A The representative images of γH2A.X expression in HOKs treated with the different

concentrations of arecoline (blue: DAPI, red: γH2A.X, γH2A.X positive cell: white arrow). **B**

The proportion of γH2A.X positive cells in HOKs treated with differentiation concentrations of

arecoline. **C** The representative images of the senescent HOK (blue: DAPI, red: γH2A.X). *$p <$

0.05, ** $p < 0.01$, *** $p < 0.001$, **** $p < 0.0001$. Scale bar: 100μm in 100×, 50μm in 200×.

(A)

DAPI γH2A.X Merge

HOK cells

NC

20 µg/ml

40 µg/ml

80 µg/ml

160 µg/ml

320 µg/ml

(B)

Percentage of γH2A.X⁺ cell

0 µg/ml 20 µg/ml 40 µg/ml 80 µg/ml 160 µg/ml 320 µg/ml

(C)

Brightfield DAPI

Senecent HOK cell

γH2A.X Merge
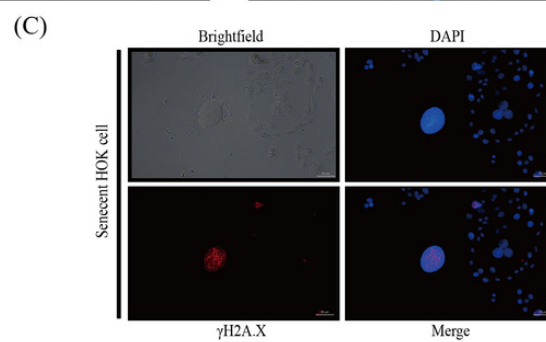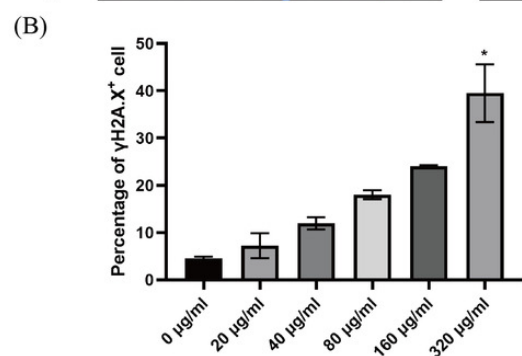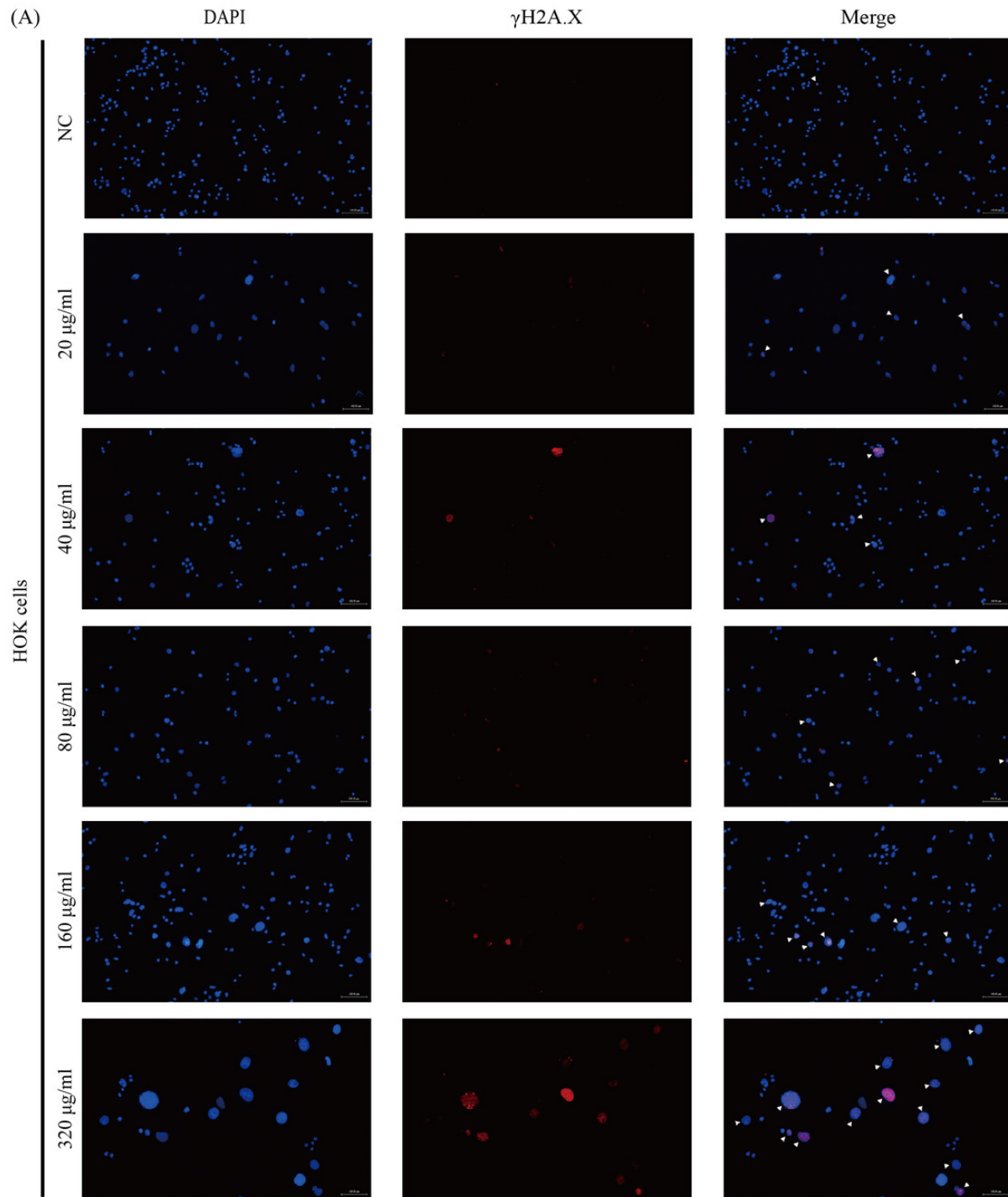
Figure 4

The expressions of p16, p21, p53, and TGF-β1 in HOKs treated with 0μg/ml arecoline or 320 μg/ml arecoline after senescence induction.

A The representative images of p16, p21, p53, TGF-β1, and GAPDH protein levels in HOKs treated with 0 μg/ml or 320 μg/ml arecoline. **B** Quantification expressions of p21 at protein and mRNA levels in HOKs treated with 0 μg/ml or 320 μg/ml arecoline. **C** Quantification expressions of p53 at protein and mRNA levels in HOKs treated with 0 μg/ml or 320 μg/ml arecoline. **D** Quantification expressions of TGF-β1 at protein and mRNA levels in HOKs treated with 0 μg/ml or 320 μg/ml arecoline. **E** TGF-β1 expression in supernatants of HOKs treated with 0 μg/ml or 320 μg/ml arecoline. *$p < 0.05$, ** $p < 0.01$, *** $p < 0.001$, **** $p < 0.0001$.
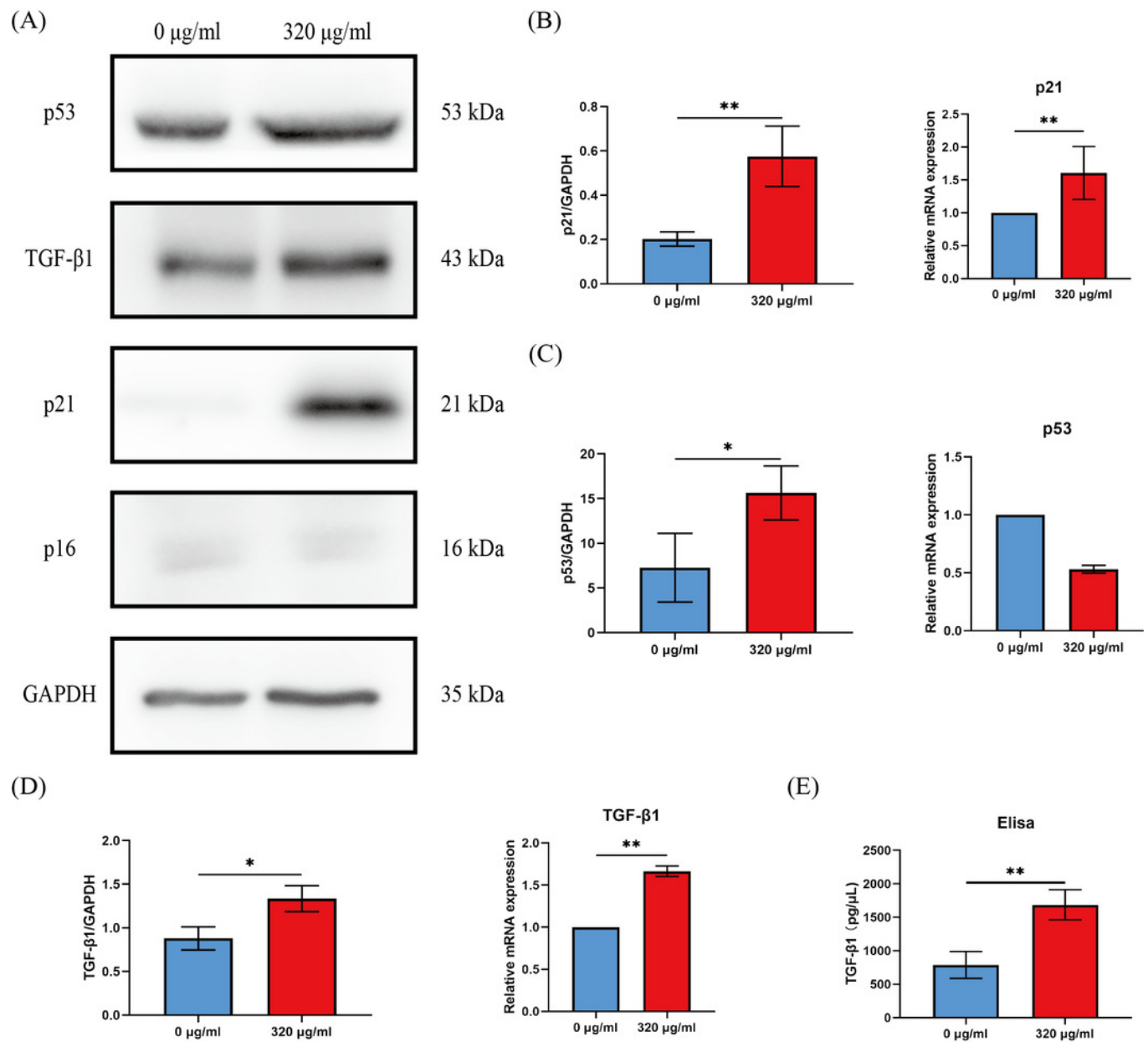
(A)

0 µg/ml   320 µg/ml

p53   53 kDa

TGF-β1   43 kDa

p21   21 kDa

p16   16 kDa

GAPDH   35 kDa

(B)

(C)

(D)

(E)

Figure 5

The mechanism diagram for the role of senescent epithelial cells in the development of OSF.

Table-revision

1 Table 1 Primer sequences used in this study.

Name	Sequence	Tm value
p16	F 5'-GGGTTTTCGTGGTTCACATCC-3'	55.10
	R 5'-CTAGACGCTGGCTCCTCAGTA-3'	60.77
p21	F 5'-TGTCCGTCAGAACCCATGC-3'	56.22
	R 5'-AAAGTCGAAGTTCCATCGCTC-3'	57.38
p53	F 5'-CAGCACATGACGGAGGTTGT-3'	57.6
	R 5'-TCATCCAAATACTCCACACGC-3'	55.79
TGF-β1	F 5'-CTAATGGTGGAAACCCACAACG-3'	56.50
	R 5'-TATCGCCAGGAATTGTTGCTG-3'	57.77
GAPDH	F 5'-CCATGGGTGGAATCATATTGGA-3'	57.60
	R 5'-TCAACGGATTTGGTCGTATTGG-3'	58.11